Regulation of oxytocin-induced calcium transients and gene expression in engineered myometrial tissues by tissue architecture and matrix rigidity

Antonina P. Maxey[1], Jaya M. Travis[1], Megan L. McCain[1,2*]

AFFILIATIONS

[1]Laboratory for Living Systems Engineering, Alfred E. Mann Department of Biomedical Engineering, USC Viterbi School of Engineering, University of Southern California, Los Angeles, CA, USA

[2]Department of Stem Cell Biology and Regenerative Medicine, Keck School of Medicine of USC, University of Southern California, Los Angeles, CA, USA

mlmccain@usc.edu*

ABSTRACT

The uterus is susceptible to benign tumors known as fibroids, which have been associated with many pregnancy complications, including preterm labor. However, the impact of fibrotic tissue remodeling on the physiology of the myometrium, the smooth muscle layer of the uterus, is poorly understood, in large part due to a lack of model systems. In this study, we engineered healthy-like and fibrotic-like myometrium by culturing human myometrial smooth muscle cells on polyacrylamide hydrogels micropatterned with fibronectin to independently tune matrix rigidity and tissue alignment, respectively. We then evaluated calcium transients in response to oxytocin stimulation. Isotropic myometrial tissues on stiff substrates (representing fibrotic myometrium) had shorter calcium transients due to shorter decay time compared to aligned myometrial tissues on soft substrates (representing healthy myometrium). Calcium transients in aligned tissues had longer response times and longer decay times than isotropic tissues, irrespective of substrate stiffness. The amplitude of calcium transients was also higher on soft substrates compared to stiff substrates, irrespective of tissue alignment. We also performed RNA sequencing to detect differentially expressed genes between healthy- and fibrotic-like tissues, which revealed that a bitter taste receptor shown to induce smooth muscle relaxation, *TAS2R31,* was down-regulated in fibrotic-like tissues. Finally, we measured oxytocin-induced calcium transients in response to pre-treatment with progesterone, caffeine, thrombin, and nifedipine to demonstrate applications for our model system in drug screening. Both progesterone and caffeine caused a decrease in calcium transient duration, as expected, while thrombin and nifedipine had less impact. Collectively, our engineered model of the myometrium enables new insights into myometrial mechanobiology and can be extended to identify or screen novel drug targets.

KEYWORDS: calcium, myometrium, micropattern, pregnancy, fibroid, labor

1. Introduction

Uterine contractions are generated by the smooth muscle cells in the middle layer of the uterus, known as the myometrium. Healthy myometrium consists of circularly or longitudinally aligned muscle layers[1,2] with an elastic modulus of 10-30 kPa[3,4], depending on the measurement technique. Fibrotic regions or fibroids are prevalent in 4.5 - 68.6% of women[5] and are associated with abnormal uterine contractions in non-pregnant women, which may contribute to infertility[6]. Uterine fibroids also affect 2-10% of pregnant women[7] and have been associated with complications such as preterm labor[8] and Caesarean section[4,9]. Structural evaluation of the extracellular matrix (ECM) in fibroids has shown random orientations of collagen fibrils[10] and a two to four-fold increase in tissue stiffness[4,11], which may contribute to preterm labor by reducing the distension threshold required to initiate labor or causing ill-timed contractions[12]. Preterm labor, defined as labor that begins prior to 37 weeks of gestation, almost always leads to preterm birth, the leading cause of neonate death[13]. Current interventions for preterm labor are limited and include administration of tocolytics, a class of drugs that temporarily delay labor[14]. However, most tocolytics, such as nifedipine, a beta-2 adrenergic receptor agonist, are non-specific and can cause many adverse side effects for both the mother and fetus[15-17]. Fibroids can also decrease the force of contractions or disrupt the coordination between cells, resulting in dysfunctional labor[12], Caesarean section[18], or postpartum hemorrhage[19]. Caesarean sections also cause uterine scarring and increased matrix deposition, which can result in dysmenorrhea for non-pregnant women[20] and increase the risk for preterm labor in future pregnancies[21]. The overall impact of fibroids on childbirth is likely to increase because fibroid incidence increases with age[22] and the median age of childbirth increased by three years between 1990 and 2019[23]. Thus, there is a significant clinical need to better understand relationships between fibrosis and myometrial smooth muscle cell physiology.

Although studies have shown that substrate stiffness modulates contractile phenotypes in vascular smooth muscle cells[24], the impact of matrix stiffness on myometrial smooth muscle cells remains poorly understood. This is partly due to a lack of model systems, which are generally limited to: animal models (mostly rodents) that are fundamentally incapable of recapitulating many unique features of human parturition[25]; or explanted human tissue strips collected during elective Caesarean sections, which are rare, difficult to prepare and maintain, and suffer from low reproducibility[26]. Human *in vitro* models, which are relatively accessible and reproducible, have also been generated by culturing human myometrial smooth muscle cells as a monolayer or engineered tissue ring[27]. However, evaluating the physiological effects of fibrotic-like conditions on human myometrial cells in a controlled *in vitro* setting has not yet been attempted, limiting our understanding of the direct impact of fibrotic tissue remodeling on myometrial function.

To address these knowledge gaps in myometrial mechanobiology, our goal was to engineer an *in vitro* system for directly measuring the effects of tissue architecture and matrix rigidity on the structure, physiology, and transcriptome of human myometrium. To mimic healthy and fibrotic myometrium, we adapted our previous techniques[28] for microcontact printing fibronectin onto polyacrylamide hydrogels to garner independent control over tissue alignment and matrix rigidity. We then cultured primary human myometrial smooth muscle cells on these hydrogels and characterized tissue structure and identified differentially expressed genes via RNA sequencing. We also evaluated calcium transient morphology in response to oxytocin stimulation, revealing unique effects of matrix rigidity and tissue alignment on calcium

dynamics. Lastly, we evaluated the effects of several compounds, including nifedipine, on oxytocin-induced calcium transients to serve as a proof-of-concept demonstration of our assay for applications in compound screening. Collectively, our engineered model of the myometrium enables new insights into myometrial mechanobiology and can also be used to identify novel drug targets and screen the functional effects of compounds.

2. Methods

2.1 Substrate preparation

Polyacrylamide hydrogels were fabricated according to previous methods[29,30]. Briefly, solutions of 40% acrylamide (Bio-Rad) and 2% N,N'-methylenebisacrylamide (Sigma-Aldrich) were combined with water, ammonium persulfate, and TEMED using indicated ratios for 13 kPa or 90 kPa elastic modulus. The solution was combined with streptavidin acrylamide (1:6 dilution), then 20 μL of the resulting solution was pipetted onto 25 mm glass coverslips activated with sodium hydroxide, APTES, and glutaraldehyde[29]. Non-activated 18 mm glass coverslips were placed atop the solution to flatten the polyacrylamide drop. The hydrogels were cured at room temperature for 30 minutes, then the non-activated 18 mm coverslips were removed under sterile conditions using a razor blade. Cured hydrogels were rinsed three times with PBS then stored at 4°C in PBS for up to one week.

Hydrogels were microcontact printed with biotinylated fibronectin in either aligned or isotropic patterns per previously described methods[29,31] (Fig. 1A). Polydimethylsiloxane (PDMS) stamps were cast on wafer templates prepared using standard photolithography[32]. Wafer templates were either un-patterned (for isotropic) or patterned with 40 μm wide rows separated by 75 μm wide gaps (for aligned). Biotinylated fibronectin was prepared by incubating biotin (Thermo), fibronectin (Corning), and sodium carbonate overnight, then dialyzing against PBS to remove un-reacted biotin, similar to previously published protocols[30]. Feature-less PDMS stamps were submerged in 95% ethanol, sonicated for 30 minutes, dried with compressed air under sterile conditions, coated with biotinylated fibronectin, and incubated for at least one hour. Simultaneously, polyacrylamide hydrogels were dried for 30 minutes in a desktop incubator at 37°C. Excess fibronectin was removed from the PDMS stamps, then stamps were dried with compressed air. For isotropic samples, the dried PDMS stamps were placed directly on the dried polyacrylamide hydrogels with light pressure. For aligned samples, a UVO-treated (8 min) lane template stamp was used to selectively remove biotinylated fibronectin from a flat PDMS stamp, resulting in 40 μm wide lanes; the flat PDMS stamp was then placed onto the polyacrylamide hydrogel with light pressure. Stamps remained in contact with the gel for approximately six minutes before the stamp was removed and the coverslip was rinsed three times with PBS. Microcontact printed hydrogels were stored at 4°C then seeded within hours of stamping.

2.2 Cell culture

Cell culture media was prepared by combining vascular cell basal medium (ATCC PCS-100-030), vascular smooth muscle cell growth kit (ATCC PCS-100-042), and penicillin-streptomycin (0.1%) and then sterilizing with a 0.22 μm vacuum filter. Primary human uterine smooth muscle cells (HUtSMC, ATCC PCS-460-011) were received at passage two (batch #62232441) and stored in liquid nitrogen. T75 flasks were coated with 0.1% gelatin (Stem Cell Technologies) at 37°C for 30 minutes, followed by incubation with warm media for an additional

30 minutes. The cell vial was then thawed in a water bath, resuspended in warm media, and divided between three gelatin-coated T75 flasks. Cells were maintained at 37°C, 5% CO_2 and media was replenished after two days. Cells were passaged using trypsin on the third day (approximately 75% confluence) into nine T75 gelatin-coated flasks. On the fifth day, cells were passaged, resuspended in freezing media (media supplemented with 10% FBS and 10% DMSO), distributed into cryovials, and cryopreserved in liquid nitrogen. For experiments, a single cryovial was similarly thawed and expanded in gelatin-coated T75 flasks. Cells were then detached from flasks and seeded at a density of 125,000 cells per 2 mL media on microcontact-printed polyacrylamide hydrogel coverslips in a 6-well plate. All measurements were collected within four days of seeding at passage five.

2.3 Immunochemistry and structural quantification

After two days of culture, coverslips were rinsed with PBS and fixed and permeabilized with paraformaldehyde (4%) and Triton (0.1%), respectively, for ten minutes. Coverslips were then rinsed three times with PBS and stored at 4°C for a maximum of one week.

Primary staining was performed by inverting coverslips on droplets of PBS with anti-fibronectin antibody produced in rabbit (Sigma, 1:200) for 1.5 hrs followed by three PBS rinses. For secondary staining, coverslips were incubated with goat anti-rabbit antibody conjugated to Alexa Fluor 546 (Life Technologies, 1:200), DAPI (1:200), and phalloidin conjugated to Alexa Fluor 488 (Life Technologies, 1:200) for 1.5 hours. Coverslips were then rinsed three times with PBS, slightly dried, inverted onto 30 µL of ProLong Gold Antifade (Life Technologies) on a glass slide, and sealed with nail polish.

Samples were imaged with a Nikon C2 point-scanning confocal fluorescent microscope with a 60x oil (NA=1.515) objective with a minimum of five field of view per coverslip. For each coverslip, actin coherency was quantified using the phalloidin stain and the ImageJ plugin, OrientationJ [33]. Five fields of view per coverslip were stitched together and coherency was calculated for the stitched image. To calculate cell density, the number of nuclei in each field of view (based on the DAPI stain) was quantified and averaged using CellProfiler and then divided by an estimate of the fibronectin surface area coverage. CellProfiler was also used to measure the average major and minor axes and aspect ratio of the nuclei for each coverslip. Each datapoint represents one coverslip, with a total n=5 coverslips. All data was statistically compared with one-way ANOVA, Dunnet's or Tukey's multiple comparisons test in Graphpad Prism.

2.4 Live imaging and analysis of calcium transients

Oxytocin powder (Sigma Aldrich) was reconstituted with PBS and stored at -20°C in 2 ug/uL stock aliquots. Immediately before experiments, aliquots were warmed and added to Tyrode's solution (5.0 mM HEPES, 1.0 mM magnesium chloride, 5.4 mM potassium chloride, 135.0 mM sodium chloride, 0.33 mM potassium phosphate, 1.8 mM calcium chloride, 5.0 mM D-glucose, pH 7.4 at 37°C).

Fluo-4 AM calcium-sensitive dye (Invitrogen) was reconstituted in Pluronic-127, added to media for a final concentration of 1.7 µg/mL, then added to a coverslip well to incubate for 40 minutes. Samples were then rinsed with 37°C Tyrode's solution three times to remove unincorporated Fluo-4, then placed in the 37°C microscope incubation chamber with 1 mL Tyrode's solution to acclimate for 10 minutes prior to experimentation.

Fluo-4 fluorescence intensity and brightfield images were collected over the course of three minutes using a 20x objective lens and an Andor Zyla sCMOS camera at two frames per

second. Oxytocin solutions (0.001, 0.01, 0.1, 1 g/L) were added at the 50 second timepoint. Drug response studies followed a similar protocol while also adding the drug prior to oxytocin. Incubation times for each drug were based on previous studies and varied by drug to account for mechanism of action. Progesterone (5 μg/mL) was added 24-36 hours before calcium imaging. Caffeine (5mM)[34] and thrombin (1 U/mL)[35] were added to the Tyrode's at the start of the chamber acclimation for a total of 15 minutes before imaging. Nifedipine (5 μg/mL) was added to the media during Fluo-4 incubation for a total of 40 minutes before rinsing with Tyrode's solution and imaging[36].

For each video, fluorescence intensity of manually selected ROIs (4x4 pixels, in cytoplasm) was measured for each timepoint using Matlab. ROIs were manually excluded if no value exceeded the baseline established in the first 50 seconds or if spontaneous contractions occurred between 40-120 seconds. All ROIs for one coverslip were averaged, representing n=1.

Each transient was evaluated for amplitude[37] and time dynamics including response time[38,39], tau decay constant[39], and duration[39,40] by modifying custom Matlab software[41,42]. Response time is the time between the addition of oxytocin and the maximum fluorescence intensity. Decay is the time between the maximum and 36% of the maximum on the downstroke. Duration spans the time at half of the maximum on the upstroke to the same value on the downstroke. Amplitude is the maximum normalized to the baseline. All ROI results from one sample were averaged to represent that coverslip as n=1. Each condition includes coverslips from different experimental batches and days. All data was evaluated with one-way or two-way ANOVA and Tukey's multiple comparisons test in Graphpad Prism.

2.5 Gene expression analysis

Cells from different experimental batches were lysed and RNA was isolated using Qiagen miRNeasy Micro kits per the manufacturer's protocol. Briefly, chloroform was added to cell-Qiazol homogenate for phase separation. The upper aqueous phase was mixed with ethanol, then repeatedly filtered through a spin column with buffer solution and diluted ethanol. RNA was passed through an additional cleaning step (Zymo RNA Clean and Concentrator) then eluted with RNase-free water before storing at -80°C prior to sequencing with an Illumina NovaSeq 6000 (performed by Novogene Corporation, Inc.).

Analyses were performed using Partek Flow Genomic Analysis software. Sequenced reads were trimmed from both ends based on a Phred quality score of 20 and a minimum read length of 25 remaining bases then aligned with the STAR algorithm to the hg38 genome. Data was filtered and normalized with the median ratio, then differentially expressed genes were identified with DESeq as p-value <0.01 and fold change greater than the absolute value of 2. Likely due to sample-to-sample variability, we did not observe genes with statistically significant FDR. RNA-seq data were submitted to the National Center for Biotechnology Information (NCBI) Gene Expression Omnibus (GEO) data repository (accession number GSE233288; n =8 isotropic 13 kPa, n = 8 aligned 13 kPa, n = 8 isotropic 90 kPa, n = 8 aligned 90 kPa).

3. Results

3.1 Engineering models of healthy and fibrotic human myometrium

In a healthy uterus, myometrial tissue is aligned and relatively compliant, with an elastic modulus of approximately 10-30 kPa[3,4]. Fibrotic myometrial tissue is less organized and stiffer,

with a two to four-fold increase in tissue stiffness[4,11]. To determine the effects of fibrotic remodeling on myometrial structure and function, we used our previously established techniques[28,30] to engineer polyacrylamide hydrogels with elastic moduli of 13 kPa and 90 kPa. We then microcontact printed fibronectin onto these hydrogels as a uniform coating or as 40 μm-wide lanes separated by 75 μm gaps (Fig 1A). Next, we seeded primary human myometrial smooth muscle cells on the hydrogels, cultured them for two days, and stained for nuclei, actin filaments, and fibronectin (Fig 1B). The number of nuclei per field of view normalized to fibronectin area was not statistically different between conditions (Fig 1C), indicating consistent cell adhesion and viability. Nuclei aspect ratio was significantly higher in aligned tissues compared to isotropic tissues on 13 kPa hydrogels. Nuclei aspect ratio trended higher in aligned tissues compared to isotropic tissues on 90 kPa hydrogels but did not reach statistical significance (Fig 1D). The coherency of actin filaments, which ranges from zero for disordered systems to one for oriented or coherent systems, was significantly higher in aligned tissues compared to their isotropic counterparts (Fig 1E), as expected. Together, these data demonstrate that we can reproducibly engineer human myometrial tissues with independent control over tissue alignment and matrix elasticity to model aspects of healthy and fibrotic tissue.

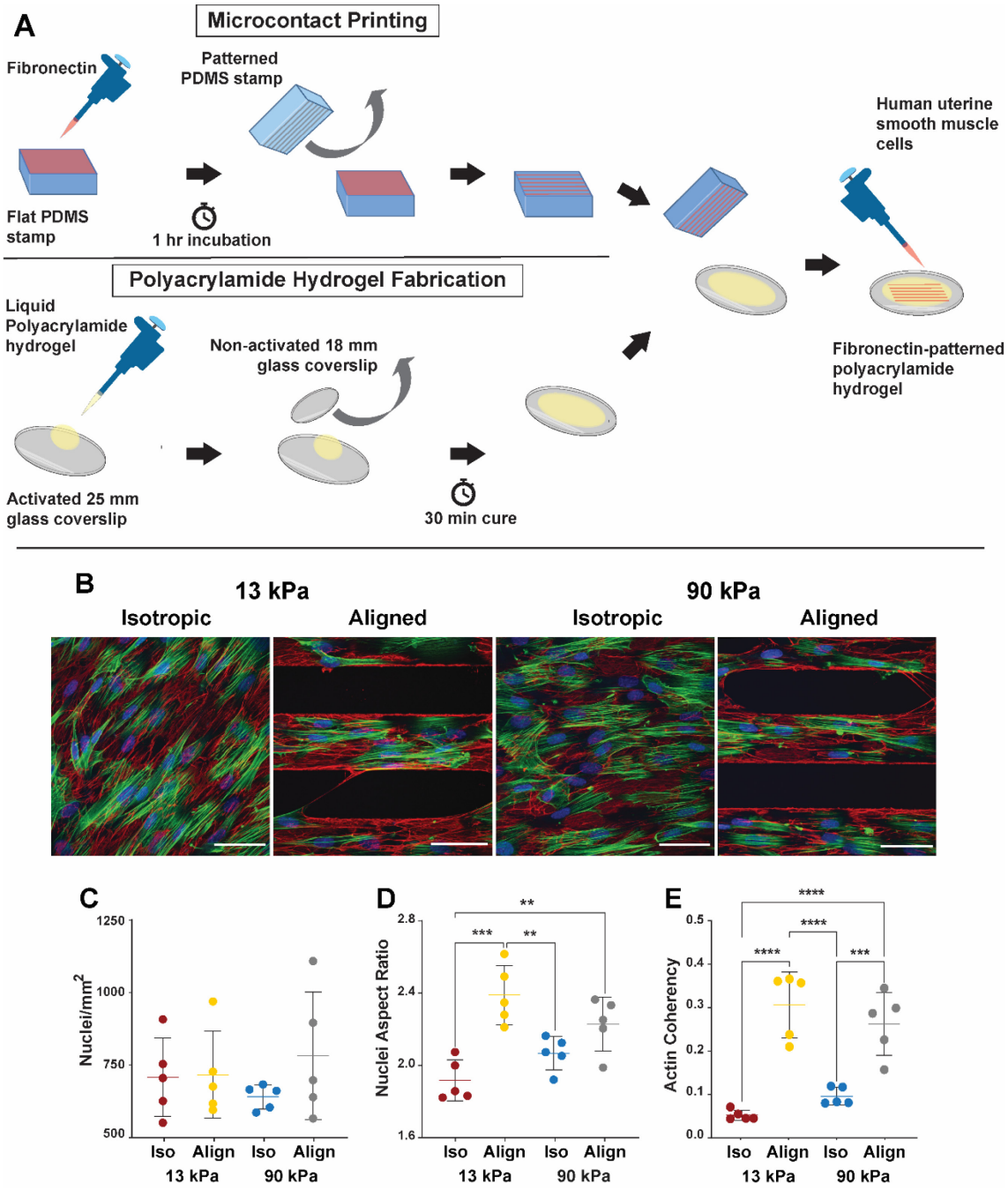

Figure 1: Structure of engineered myometrial tissues. (A) Schematic of microcontact printing and polyacrylamide hydrogel fabrication. (B) Representative fluorescent images of myometrial tissues on isotropic or aligned fibronectin micropatterns on 13 kPa or 90 kPa polyacrylamide gels. Blue: nuclei, green: F-actin, red: fibronectin. Scale bar: 50 μm. * denotes $p < 0.05$, ** $p < 0.01$, *** $p < 0.001$, **** $p < 0.0001$ using Tukey's multiple comparisons test. (C) Number of nuclei normalized to fibronectin area in field of view. (D) Nuclei length divided by width (aspect ratio). (E) Actin alignment quantified as coherency.

3.2 Dose response of calcium transients to oxytocin

Because increased intracellular calcium concentrations are correlated with increased contractile activity in muscle cells[43], we next developed a microscopy-based workflow to measure calcium activity in engineered myometrial tissues in response to oxytocin stimulation as a proxy for contractile activity. Our first goal was to establish an oxytocin dose response curve. To do so, we incubated aligned myometrial tissues on 13 kPa substrates with the fluorescent calcium indicator Fluo-4. We then captured images of Fluo-4 fluorescence for 50 seconds (rate: 2 frames per second) as a baseline (Fig 2A). We then added oxytocin at doses ranging from 10^{-4} g/L to 10^{-1} g/L, similar to the range of concentrations used clinically[44] or in previous *in vitro* studies[34]. We then continued acquisitions for a total of three minutes, which was sufficient for capturing maximum Fluo-4 intensity and return to baseline (Fig 2A). Next, we processed image stacks with custom Matlab software to produce graphical representations of Fluo-4 intensity over time in multiple regions of interest per field of view and measured the average amplitude, response time, decay, and duration of the resulting calcium transients (Fig 2B). As expected[34,45], increasing the concentration of oxytocin resulted in calcium transients with faster response time (Fig 2C), faster decay (Fig 2D), and shorter duration (Fig 2E). Amplitude also trended higher as oxytocin increased (Fig 2F), but without statistical significance. Together, these data demonstrate that calcium transients in our engineered myometrial tissues were responsive to oxytocin in a manner that trended with increasing dosage, which is the expected physiological response.

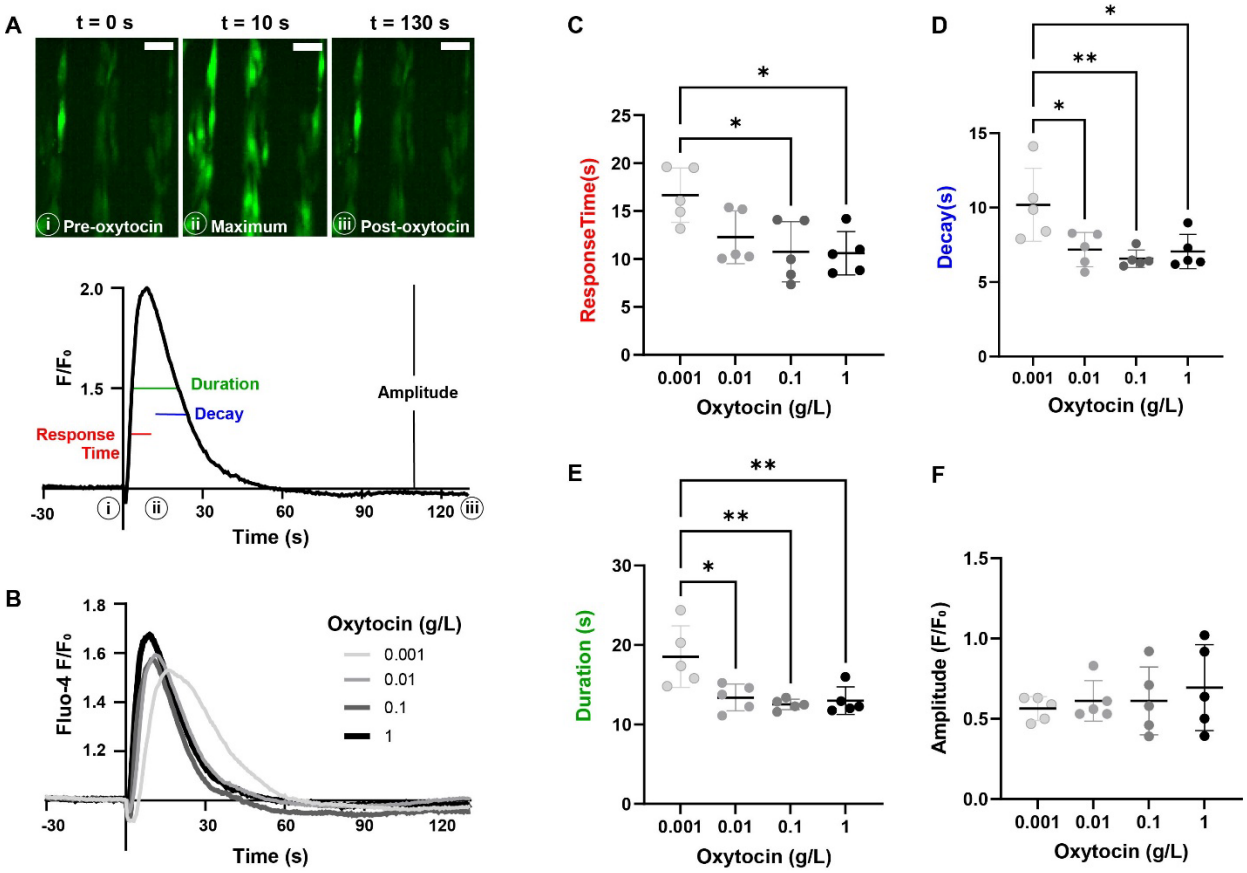

Figure 2*:* Calcium transients in response to increasing concentrations of oxytocin. (A) Representative images of baseline (t = 0 s), maximum (t = 10 s), and steady state (t = 130 s) fluorescence intensity. (B) Average calcium transients. * denotes $p < 0.05$, ** $p < 0.01$ using Tukey's multiple comparisons test. (C) Response time, (D) decay, (E) duration, and (F) amplitude dose responses to oxytocin.

3.3 Modulation of calcium transients by tissue alignment and matrix rigidity

To investigate the impact of tissue alignment and matrix rigidity on myometrial physiology, we engineered the four types of tissues shown in Figure 1 by independently modifying substrate elastic modulus (13 kPa, 90 kPa) and cell alignment. We then performed the same calcium imaging protocol shown in Figure 2 with 10^{-1} g/L oxytocin since this concentration induced a robust response (Figure 3A). We proceeded to quantify the same metrics shown in Figure 2 and compared all conditions independently with one-way ANOVA. As shown in Figure 3B, response time was slower in aligned tissues compared to isotropic tissues on 90 kPa substrates. Additionally, aligned tissues on 13 kPa substrates (the closest mimic to healthy tissue) had a longer decay (Figure 3C) and a longer duration (Figure 3D) compared to isotropic tissues on 90 kPa substrates (the closest mimic to fibrotic tissue). No significant differences in amplitude were detected (Figure 3E). We then performed a two-way ANOVA to detect any differences in calcium transients when grouping tissues solely by elastic modulus or alignment (Figure 4F). Interestingly, aligned tissues (independent of elastic modulus) had significantly longer response time, decay, and duration compared to isotropic tissues. Tissues on 13 kPa gels (independent of alignment) had significantly higher amplitude and longer decay and duration.

Together, these data suggest that fibrotic uterine tissues may have a weaker calcium response to oxytocin compared to healthy uterine tissues due to remodeling of tissue architecture and stiffness.

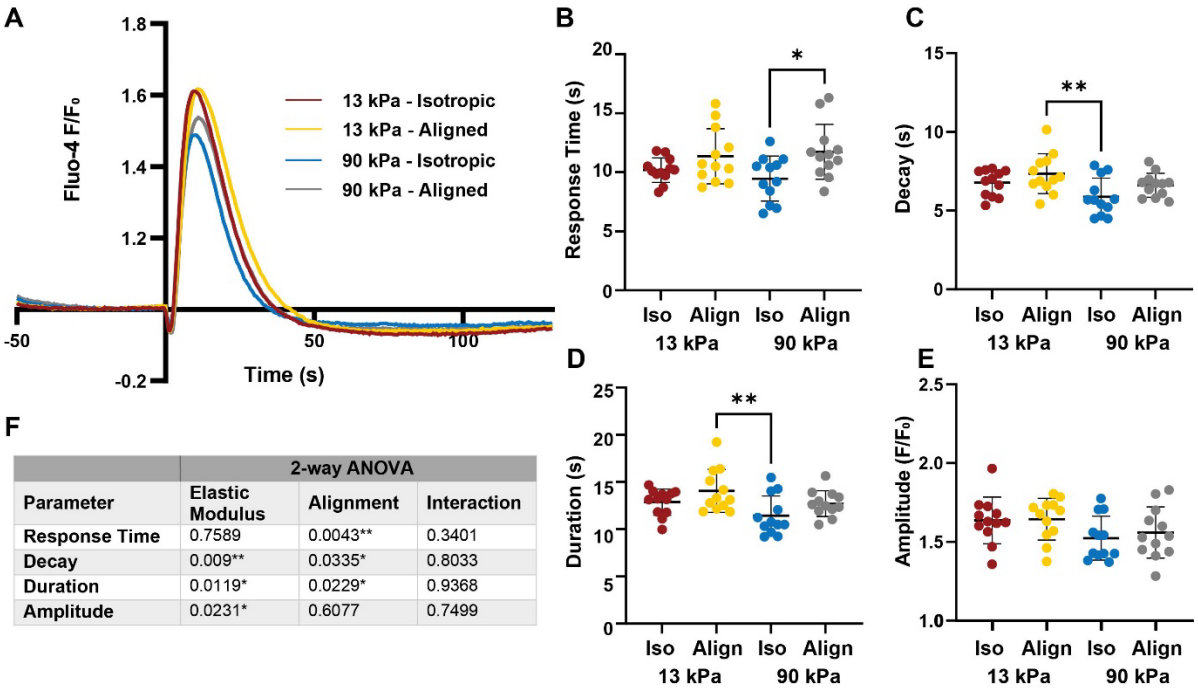

F

	2-way ANOVA		
Parameter	Elastic Modulus	Alignment	Interaction
Response Time	0.7589	0.0043**	0.3401
Decay	0.009**	0.0335*	0.8033
Duration	0.0119*	0.0229*	0.9368
Amplitude	0.0231*	0.6077	0.7499

Figure 3: Calcium transients in engineered myometrial tissues. (A) Average calcium transients for each of the four conditions. * denotes $p < 0.05$, ** $p < 0.01$ using Tukey's multiple comparisons test. (B) Response time from the addition of oxytocin to the maximum fluorescence intensity; (C) Decay time constant from the maximum to 36% of the maximum; (D) Duration as curve width at half of the maximum; (E) Normalized amplitude at maximum. (F) Two-way ANOVA analysis of calcium transient response to oxytocin as a function of elastic modulus and alignment.

3.4 Modulation of gene expression by tissue alignment and matrix rigidity

To evaluate transcriptional changes based on tissue alignment and matrix rigidity, we performed bulk RNA sequencing on myometrial cells cultured under the same conditions (13 kPa or 90 kPa hydrogels; isotropic or aligned). We compared our stiff and isotropic (90 kPa isotropic) condition (representing fibrotic tissue) to our softer and aligned (13 kPa aligned) condition (representing the healthy tissue) as a volcano plot (Fig 4A). From this plot, we listed and queried the differentially expressed genes with p-value <0.01 and fold change greater than 2 or less than -2 (Fig 4B). One of the top differentially expressed genes is *TAS2R31*, which encodes for a bitter taste receptor that is associated with airway[46] and uterine smooth muscle relaxation[47] and thus has been proposed as a target for tocolytics[48]. We further mined our data to determine if other bitter taste receptors (TAS2R) are expressed in our engineered tissues. We ultimately detected expression of fourteen other type 2 taste receptors and one type 1 receptor in our healthy- and fibrotic-like tissues (Figure 4C), consistent with other reports demonstrating that bitter taste receptors are expressed by myometrial smooth muscle cells[48].

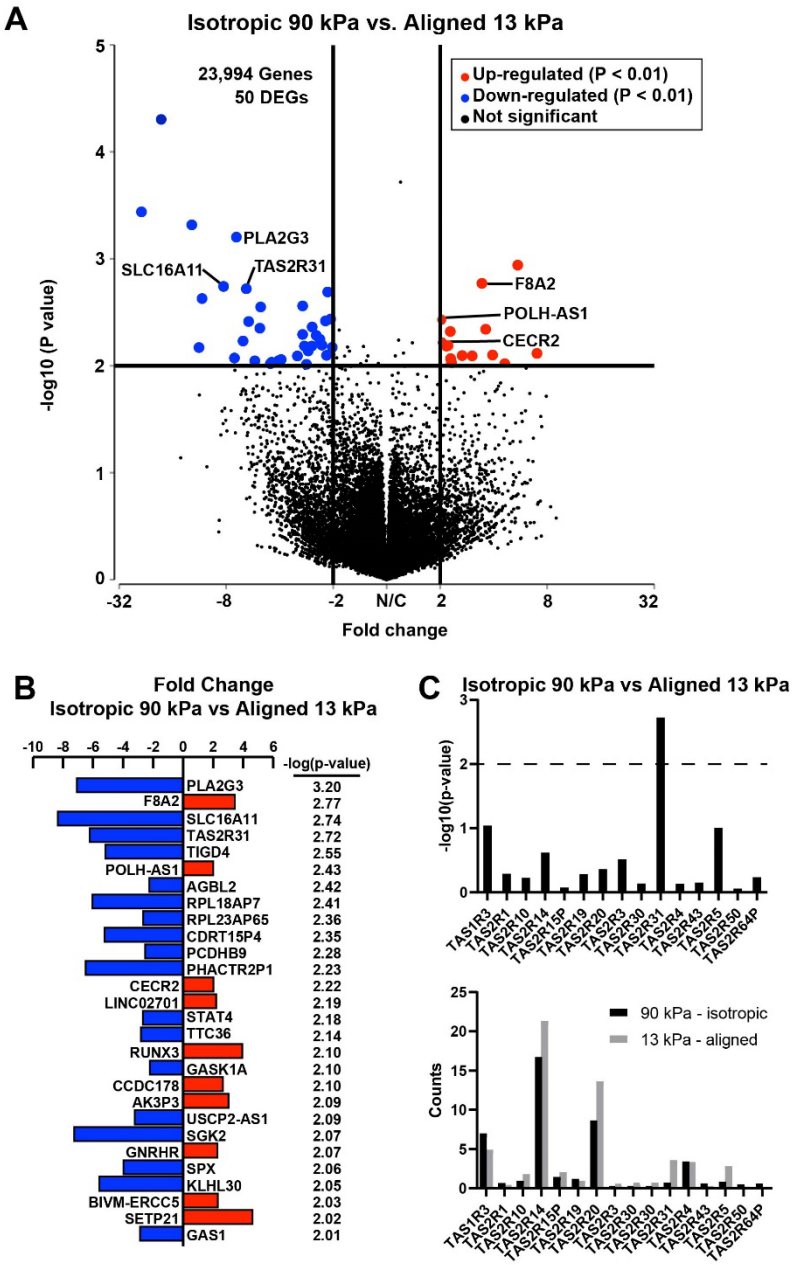

Figure 4: Transcriptomic analysis of engineered myometrial tissue (A) Volcano plot of comparison between Isotropic 90 kPa and Aligned 13 kPa with down-regulated (blue) and up-regulated (red) genes [$P < 0.01$, absolute value of the fold change (|fold change|>2). The dotted black horizontal and vertical lines identify the fold change and p-value cut offs. The DEGs are labeled by gene symbol. (B) Bar graph of fold change for significantly up or downregulated genes. (C) Bar graphs of p-value and normalized gene counts versus identified taste receptors.

3.5 Engineered myometrial tissues mimic clinical responses to compounds

Next, we asked if our engineered tissues would respond as expected to a variety of compounds known to impact the response of myometrial cells to oxytocin. For these experiments, we used aligned myometrial cells on 13 kPa substrates to most closely represent healthy tissues. We also used a relatively low dose of oxytocin (10^{-4} g/L) to ensure a measurable

range of responses. First, we tested the impact of pre-treating tissues with progesterone. Progesterone is a steroid hormone that maintains the uterus in a quiescent state throughout pregnancy[49]. Synthetic progesterone is also used as a long-term tocolytic and has been shown to reduce contractility through both non-genomic and genomic[15] mechanisms, such as reducing calcium entry[15,50] and modulating oxytocin receptor density[50], respectively. For these reasons, we incubated tissues with progesterone for 24-36 hours prior to functional testing to account for any transcriptional changes (Fig 5A). Progesterone significantly slowed the initial response to oxytocin (Fig 5B), shortened the decay time to baseline (Fig 5C), and shortened the overall duration (Fig 5D), consistent with a lessened contractile response. Although not significant, the amplitude of progesterone-treated tissues trended lower than control, also suggesting a lessened contractile response (Fig 5E).

Next, we tested the short-term effects of compounds that have previously shown to acutely impact the myometrium. Similar to progesterone, caffeine has a relaxant effect on uterine smooth muscle[34]. Conversely, the coagulation factor thrombin has been associated with preterm labor, likely through direct activation of myosin[35]. Nifedipine is an acute tocolytic uncommonly used to quell contractions in the short-term[15]. To test the effects of caffeine and thrombin, we added caffeine or thrombin to Tyrode's solution, for a total of 15 minutes incubation time before imaging; nifedipine was added at the start of Fluo-4 incubation for a total of 40 minutes before imaging[36] (Figure 5A) to align with previous studies[34 35]. Caffeine-treated tissues exhibited shorter decay time and shorter duration, similar to progesterone. Response time was slightly delayed by caffeine, but this was not statistically significant. Nifedipine delayed response time but did not affect any other parameters. Thrombin did not cause any effects, suggesting this compound does not impact calcium handling in myometrial smooth muscle cells. Together, these results demonstrate that this platform has potential applications in evaluating the efficacy and mechanisms of actions of new and existing compounds for modulating myometrial smooth muscle physiology.

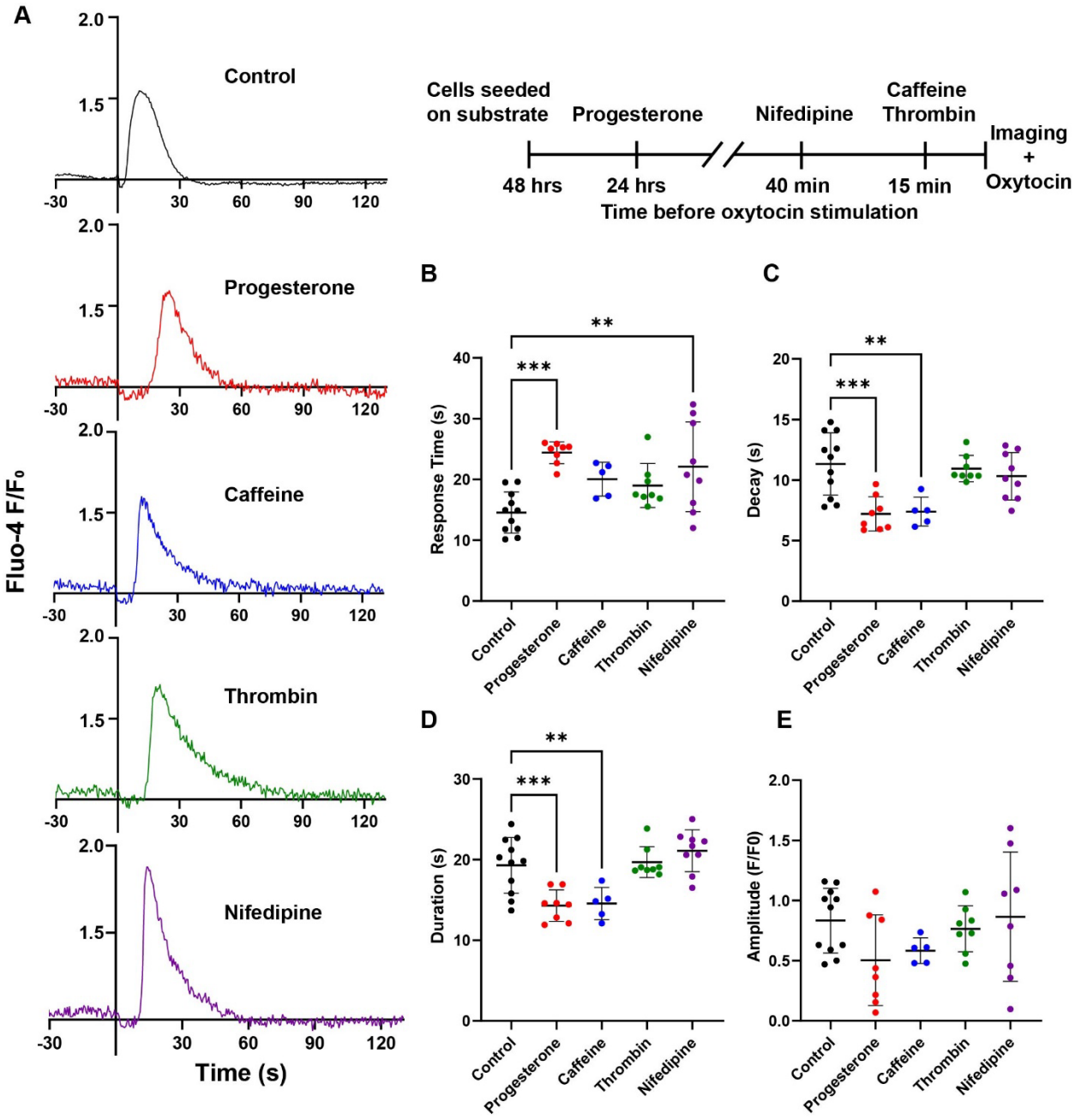

Figure 5: Drug screening in engineered myometrial tissues. (A) Representative traces of drugs used for screening and imeline of drug addition. * denotes $p < 0.05$, ** $p < 0.01$, *** $p < 0.001$ using Dunnet's multiple comparisons test. (B) Response time from the addition of oxytocin to the maximum fluorescence intensity. (C) Decay time constant from the maximum to 36% of the maximum. (D) Duration as curve width at half of the maximum. (E) Normalized amplitude at maximum.

4. Discussion

Unlike most other muscle tissues, the impact of fibrotic remodeling on myometrial smooth muscle tissue is poorly understood. To address this, we engineered a human *in vitro* model of healthy and fibrotic myometrium by culturing primary human myometrial smooth muscle cells on substrates with independently tunable matrix rigidity and cell alignment. We then characterized tissue structure, oxytocin-induced calcium transients, and the transcriptome, revealing structural, physiological, and genetic changes, respectively, caused by physical features of the tissue microenvironment. In addition, we show that our engineered myometrial tissues respond to select clinical compounds, demonstrating potential applications in drug screening.

To recreate features of the tissue microenvironment characteristic of healthy and fibrotic myometrium[1,2,10,11,51], we cultured primary myometrial smooth muscle cells on polyacrylamide hydrogels with elastic moduli of 13 kPa or 90 kPa that were then microcontact printed with fibronectin as a uniform or lane pattern. One benefit of this approach is that matrix rigidity and tissue alignment can be independently tuned, enabling their effects to be decoupled. We then seeded these substrates with human primary smooth muscle cells isolated from the myometrium. Similar to other muscle cell types[52,53], actin alignment increased on microcontact printed lanes of fibronectin compared to isotropic fibronectin. The circularity of nuclei in isotropic cells also trended lower compared to aligned cells on both 13 kPa and 90 kPa gels, which is consistent with histological data reporting that nuclei in late-stage fibroids become rounded to ovoid[54]. However, one limitation of our study is that we used purified fibronectin as the only cell adhesion protein, which does not reflect the complex composition of the extracellular matrix in healthy and fibrotic myometrium[55]. Myometrial extracellular matrix also comprises laminin and collagen and increased deposition of matrix proteins is a hallmark of fibroids[56]. Thus, future studies could evaluate matrix protein production as well as the response of myometrial cells cultured on different matrix proteins.

We next performed calcium imaging in response to oxytocin stimulation. We selected oxytocin as our contractile agonist because it has previously been used for clinical[57] and *in vitro*[15] applications and induces stronger responses compared to alternative compounds, such as prostaglandins[58]. With increasing doses of oxytocin, both the response time and decay time of calcium transients declined and thus the overall duration was shorter at higher doses of oxytocin, suggestive of faster release and uptake of intracellular calcium. Calcium transient amplitude also trended upwards with increasing oxytocin concentration, indicative of greater increases in intracellular calcium. Thus, our engineered myometrial tissues retained sensitivity to oxytocin.

To evaluate the impact of fibrotic remodeling on calcium handling, we evaluated calcium transients in engineered myometrial tissues as a function of substrate elastic modulus and tissue alignment. The duration and amplitude of calcium transients was generally highest in aligned tissues on 13 kPa gels and lowest in isotropic tissues on 90 kPa gels, which are the closest mimics of healthy and fibrotic tissues, respectively. These data suggest that fibrotic-like tissues have slower and weaker increases in intracellular calcium in response to oxytocin. To deconvolve the effects of elastic modulus and tissue alignment, we also compared calcium transient metrics using two-way ANOVA. Interestingly, aligned tissues had higher response and decay times (and thus longer durations) compared to isotropic tissues. However, tissue alignment had no impact on calcium transient amplitude. By contrast, tissues on 13 kPa gels had significantly higher calcium transient amplitude compared to those on 90 kPa gels. Tissues on 13 kPa gels also had higher decay time but no difference in response time. Thus, tissue alignment and matrix rigidity had unique impacts on calcium transient morphology.

In myometrial smooth muscle cells, calcium can enter the cytosol via L-type channels on the plasma membrane or via release from internal sarcoplasmic reticulum stores[59]. Identifying which calcium pathways and ion channels are sensitive to distinct cues in the tissue microenvironment is an important topic for further investigation to establish the mechanistic underpinnings of our data. Additionally, due to their fundamental role in mechanotransduction, the cytoskeleton or cytoskeletal mediators may link matrix remodeling to changes in myometrial physiology. For example, RhoA has been shown to be more active in leiomyoma cells cultured on rigid polystyrene compared to myometrial cells[60]. RhoA inhibits myosin light chain phosphatase, which enhances myometrial contractility[61].

To identify differentially expressed genes due to fibrotic-like tissue remodeling, we next performed bulk RNA sequencing on our tissue constructs. Because their calcium transients showed the starkest differences, we focused on comparing 13 kPa, aligned tissues to 90 kPa, isotropic tissues. This comparison revealed a relatively small number of differentially expressed genes, none of which were directly related to calcium handling. Thus, the changes we observed in calcium handling were likely not caused by changes in calcium handling proteins at the transcriptional level. In our dataset, the top differentially expressed gene was *PLA2G3,* which encodes for phospholipase A2 group III and was down-regulated in our fibrotic-like tissue compared to the healthy-like tissue. This enzyme hydrolyzes extracellular phospholipids and has been detected in vascular smooth muscle cells[62]. *SLC16A11,* which encodes for solute carrier family 16 member 11, was also down-regulated in our fibrotic-like tissues and is also involved in lipid metabolism. Thus, remodeling of the tissue microenvironment may be triggering changes in metabolism, which can also impact contractility.

The gene for *TAS2R31* was also downregulated in our fibrotic-like condition. This gene encodes for taste receptor, type 2, member 31, (TAS2R31) which is a bitter taste receptor. Bitter taste receptors (TAS2R) were initially thought to only exist on the tongue, but have also been detected in airway smooth muscle cells. Although the impact of bitter agonists on intracellular calcium in airway smooth muscle cells is variable[46,63], cells reliably exhibit relaxation or bronchodilation in response to bitter taste receptor agonists. TAS2R receptors have also been detected in uterine smooth muscle cells[47]. Consistent with these findings, we also detected the expression of fourteen TAS2R and one type 1 receptor (TAS1R) in our tissues. Bitter agonists of TAS2R (e.g., caffeine[64]) have been shown to reverse induced contractions[48] and thus have been proposed as potential targets for a new class of tocolytics. However, if TAS2R expression is down-regulated in fibrotic tissues, TAS2R agonists may have reduced tocolytic effects in these tissues. Thus, identifying if drug targets are modulated by the tissue microenvironment is an important consideration.

We also used our healthy-like tissues (13 kPa, aligned) to test responses to a variety of compounds. As expected, cells incubated with progesterone responded more slowly to oxytocin and decayed more rapidly to baseline, likely because progesterone decreased calcium entry. Similarly, caffeine resulted in a slower response to oxytocin, likely by inhibiting an increase in cAMP[1], which is a mechanism unique to smooth muscle cells. Thrombin has been shown to induce *in vitro* contractions of the myometrium, though it is likely through direct activation of myosin[35]. Thus, it follows that we did not see changes in calcium activity since this is upstream of the contractile filaments. Nifedipine, a common tocolytic, delayed the start of contraction, but the morphology of the transients did not change. Our results from this panel of compounds demonstrates that we can identify unique effects of compounds on different aspects of calcium

handling, which is important for understanding mechanisms of action of new and existing tocolytics or other categories of drugs for myometrial disorders.

In summary, we found that the tissue microenvironment can impact calcium handling in myometrial smooth muscle cells. Our functional model can be used to identify new therapeutic targets (such as bitter taste receptors) and also help identify biomarkers to predict patients who may be at higher risk for adverse labor events. Our study is limited by the inclusion of only one line of human primary myometrial smooth muscle cells. Future studies should evaluate cells from multiple patients, including those with diverse demographic backgrounds or harboring genetic mutations associated with pre-term labor or other conditions. Additionally, our engineered myometrial tissues could be integrated with other Organ on Chip models of the female reproductive system, including those that have focused on the endometrium[65], placenta[66], and ovaries[67] to evaluate cross-talk with other organs and gain a more comprehensive understanding of female reproductive physiology and pathophysiology.

5. Acknowledgements

This work was supported by the University of Southern California Annenberg and Graduate School Fellowships (APM); NSF CAREER Award CMMI 1944734 (MLM); NSF GRFP Award DGE-1842487 (APM); Center for Undergraduate Research in Viterbi Engineering (CURVE) Fellowship (JMT); the USC Viterbi School of Engineering. We acknowledge the USC Nanofabrication Core for photolithography equipment and facilities. We thank the USC Libraries Bioinformatics Service for their assistance in interpreting RNAseq data.

References

1. Wray S, Prendergast C. The Myometrium: From Excitation to Contractions and Labour. *Adv Exp Med Biol*. 2019;1124:233-263. doi:10.1007/978-981-13-5895-1_10
2. Flake GP, Moore AB, Sutton D, et al. The Life Cycle of the Uterine Fibroid Myocyte. *Curr Obstet Gynecol Rep*. Jun 2018;7(2):97-105. doi:10.1007/s13669-018-0241-7
3. Omari EA, Varghese T, Kliewer MA, Harter J, Hartenbach EM. Dynamic and quasi-static mechanical testing for characterization of the viscoelastic properties of human uterine tissue. *J Biomech*. Jul 2015;48(10):1730-6. doi:10.1016/j.jbiomech.2015.05.013
4. Acar S, Millar E, Mitkova M, Mitkov V. Value of ultrasound shear wave elastography in the diagnosis of adenomyosis. *Ultrasound*. Nov 2016;24(4):205-213. doi:10.1177/1742271X16673677
5. Marsh EE, Al-Hendy A, Kappus D, Galitsky A, Stewart EA, Kerolous M. Burden, Prevalence, and Treatment of Uterine Fibroids: A Survey of U.S. Women. *J Womens Health (Larchmt)*. Nov 2018;27(11):1359-1367. doi:10.1089/jwh.2018.7076
6. Nishino M, Togashi K, Nakai A, et al. Uterine contractions evaluated on cine MR imaging in patients with uterine leiomyomas. *Eur J Radiol*. Jan 2005;53(1):142-6. doi:10.1016/j.ejrad.2004.01.009
7. Spyropoulou K, Kosmas I, Tsakiridis I, et al. Myomectomy during pregnancy: A systematic review. *Eur J Obstet Gynecol Reprod Biol*. Nov 2020;254:15-24. doi:10.1016/j.ejogrb.2020.08.018
8. Landman AJEM, Don EE, Vissers G, et al. The risk of preterm birth in women with uterine fibroids: A systematic review and meta-analysis. *PLoS One*. 2022;17(6):e0269478. doi:10.1371/journal.pone.0269478
9. Parazzini F, Tozzi L, Bianchi S. Pregnancy outcome and uterine fibroids. *Best Pract Res Clin Obstet Gynaecol*. Jul 2016;34:74-84. doi:10.1016/j.bpobgyn.2015.11.017
10. Leppert PC, Catherino WH, Segars JH. A new hypothesis about the origin of uterine fibroids based on gene expression profiling with microarrays. *Am J Obstet Gynecol*. Aug 2006;195(2):415-20. doi:10.1016/j.ajog.2005.12.059
11. Jayes FL, Liu B, Feng L, Aviles-Espinoza N, Leikin S, Leppert PC. Evidence of biomechanical and collagen heterogeneity in uterine fibroids. *PLoS One*. 2019;14(4):e0215646. doi:10.1371/journal.pone.0215646
12. Rizk B, Khalaf Y, A. Borahay M. Botros R.M.B. Rizk YKMAB, ed. *Fibroids and reproduction*. CRC Press, Taylor & Francis Group,; 2021:1 online resource. https://libproxy.usc.edu/login?url=https://www.taylorfrancis.com/books/9780203728987
13. Simhan HN. Preterm birth is the leading cause of neonatal mortality and is responsible for roughly one-half of long-term neurologic sequelae. *Am J Obstet Gynecol*. May 2010;202(5):407-8. doi:10.1016/j.ajog.2010.03.027
14. Haas DM, Benjamin T, Sawyer R, Quinney SK. Short-term tocolytics for preterm delivery - Current perspectives. 2014.
15. Arrowsmith S, Kendrick A, Wray S. Drugs acting on the pregnant uterus. *Obstet Gynaecol Reprod Med*. Aug 2010;20(8):241-247. doi:10.1016/j.ogrm.2010.05.001
16. Lamont CD, Jørgensen JS, Lamont RF. The safety of tocolytics used for the inhibition of preterm labour. *Expert Opin Drug Saf*. Sep 2016;15(9):1163-73. doi:10.1080/14740338.2016.1187128
17. Kim SH, Riaposova L, Ahmed H, et al. Oxytocin Receptor Antagonists, Atosiban and Nolasiban, Inhibit Prostaglandin F. *Sci Rep*. Apr 08 2019;9(1):5792. doi:10.1038/s41598-019-42181-2
18. Zhang J, Bricker L, Wray S, Quenby S. Poor uterine contractility in obese women. *BJOG*. Mar 2007;114(3):343-8. doi:10.1111/j.1471-0528.2006.01233.x

19. Oyelese Y, Ananth CV. Postpartum hemorrhage: epidemiology, risk factors, and causes. *Clin Obstet Gynecol*. Mar 2010;53(1):147-56. doi:10.1097/GRF.0b013e3181cc406d
20. Ewies AAA, Zanetto U. Caesarean section scar causes myometrial hypertrophy with subsequent heavy menstrual flow and dysmenorrhoea. *Med Hypotheses*. Oct 2017;108:54-56. doi:10.1016/j.mehy.2017.08.006
21. Williams C, Fong R, Murray SM, Stock SJ. Caesarean birth and risk of subsequent preterm birth: a retrospective cohort study. *BJOG*. May 2021;128(6):1020-1028. doi:10.1111/1471-0528.16566
22. Lou Z, Huang Y, Li S, et al. Global, regional, and national time trends in incidence, prevalence, years lived with disability for uterine fibroids, 1990-2019: an age-period-cohort analysis for the global burden of disease 2019 study. *BMC Public Health*. May 19 2023;23(1):916. doi:10.1186/s12889-023-15765-x
23. Stable Fertility Rates 1990-2019 Mask Distinct Variations by Age (2022).
24. Polio SR, Stasiak SE, Jamieson RR, Balestrini JL, Krishnan R, Parameswaran H. Extracellular matrix stiffness regulates human airway smooth muscle contraction by altering the cell-cell coupling. *Sci Rep*. 07 02 2019;9(1):9564. doi:10.1038/s41598-019-45716-9
25. Mitchell BF, Taggart MJ. Are animal models relevant to key aspects of human parturition? *Am J Physiol Regul Integr Comp Physiol*. Sep 2009;297(3):R525-45. doi:10.1152/ajpregu.00153.2009
26. Arrowsmith S, Keov P, Muttenthaler M, Gruber CW. Contractility Measurements of Human Uterine Smooth Muscle to Aid Drug Development. *J Vis Exp*. 01 2018;(131)doi:10.3791/56639
27. Souza GR, Tseng H, Gage JA, et al. Magnetically Bioprinted Human Myometrial 3D Cell Rings as A Model for Uterine Contractility. *Int J Mol Sci*. Mar 2017;18(4)doi:10.3390/ijms18040683
28. Ariyasinghe NR, Reck CH, Viscio AA, et al. Engineering micromyocardium to delineate cellular and extracellular regulation of myocardial tissue contractility. 2017;doi:10.1039/c7ib00081b
29. Rexius-Hall ML, Ariyasinghe NR, McCain ML. Engineering Shape-Controlled Microtissues on Compliant Hydrogels with Tunable Rigidity and Extracellular Matrix Ligands. *Methods Mol Biol*. 2021;2258:57-72. doi:10.1007/978-1-0716-1174-6_5
30. McCain ML, Lee H, Aratyn-Schaus Y, Kleber AG, Parker KK. Cooperative coupling of cell-matrix and cell-cell adhesions in cardiac muscle. *Proc Natl Acad Sci U S A*. Jun 19 2012;109(25):9881-6. doi:10.1073/pnas.1203007109
31. Desai RA, Rodriguez NM, Chen CS. "Stamp-off" to micropattern sparse, multicomponent features. *Methods Cell Biol*. 2014;119:3-16. doi:10.1016/B978-0-12-416742-1.00001-9
32. Qin D, Xia Y, Whitesides GM. Soft lithography for micro- and nanoscale patterning. *Nat Protoc*. Mar 2010;5(3):491-502. doi:10.1038/nprot.2009.234
33. Fonck E, Feigl GG, Fasel J, et al. Effect of aging on elastin functionality in human cerebral arteries. *Stroke*. Jul 2009;40(7):2552-6. doi:10.1161/STROKEAHA.108.528091
34. Burghardt RC, Barhoumi R, Sanborn BM, Andersen J. Oxytocin-induced Ca2+ responses in human myometrial cells. *Biol Reprod*. Apr 1999;60(4):777-82. doi:10.1095/biolreprod60.4.777
35. Nishimura F, Mogami H, Moriuchi K, Chigusa Y, Mandai M, Kondoh E. Mechanisms of thrombin-Induced myometrial contractions: Potential targets of progesterone. *PLoS One*. 2020;15(5):e0231944. doi:10.1371/journal.pone.0231944
36. Santos S, Haslinger C, Mennet M, von Mandach U, Hamburger M, Simões-Wüst AP. Bryophyllum pinnatum enhances the inhibitory effect of atosiban and nifedipine on human myometrial contractility: an in vitro study. *BMC Complement Altern Med*. Nov 04 2019;19(1):292. doi:10.1186/s12906-019-2711-5

37. Herington JL, Swale DR, Brown N, et al. High-Throughput Screening of Myometrial Calcium-Mobilization to Identify Modulators of Uterine Contractility. *PLoS One*. 2015;10(11):e0143243. doi:10.1371/journal.pone.0143243
38. Grespan E, Martewicz S, Serena E, Le Houerou V, Rühe J, Elvassore N. Analysis of Calcium Transients and Uniaxial Contraction Force in Single Human Embryonic Stem Cell-Derived Cardiomyocytes on Microstructured Elastic Substrate with Spatially Controlled Surface Chemistries. *Langmuir*. Nov 22 2016;32(46):12190-12201. doi:10.1021/acs.langmuir.6b03138
39. Halaidych OV, Mummery CL, Orlova VV. Quantifying Ca. *Biochem Biophys Res Commun*. May 21 2019;513(1):112-118. doi:10.1016/j.bbrc.2019.03.143
40. Ahola A, Pölönen RP, Aalto-Setälä K, Hyttinen J. Simultaneous Measurement of Contraction and Calcium Transients in Stem Cell Derived Cardiomyocytes. *Ann Biomed Eng*. Jan 2018;46(1):148-158. doi:10.1007/s10439-017-1933-2
41. Petersen AP, Lyra-Leite DM, Ariyasinghe NR, et al. Microenvironmental Modulation of Calcium Wave Propagation Velocity in Engineered Cardiac Tissues. *Cell Mol Bioeng*. Oct 2018;11(5):337-352. doi:10.1007/s12195-018-0522-2
42. Petersen AP, Cho N, Lyra-Leite DM, et al. Regulation of calcium dynamics and propagation velocity by tissue microstructure in engineered strands of cardiac tissue. *Integr Biol (Camb)*. Mar 6 2020;12(2):34-46. doi:10.1093/intbio/zyaa003
43. Hill-Eubanks DC, Werner ME, Heppner TJ, Nelson MT. Calcium signaling in smooth muscle. *Cold Spring Harb Perspect Biol*. Sep 01 2011;3(9):a004549. doi:10.1101/cshperspect.a004549
44. Uvnäs-Moberg K, Ekström-Bergström A, Berg M, et al. Maternal plasma levels of oxytocin during physiological childbirth - a systematic review with implications for uterine contractions and central actions of oxytocin. *BMC Pregnancy Childbirth*. Aug 09 2019;19(1):285. doi:10.1186/s12884-019-2365-9
45. Kim SH, Riaposova L, Ahmed H, et al. Oxytocin Receptor Antagonists, Atosiban and Nolasiban, Inhibit Prostaglandin F 2α -induced Contractions and Inflammatory Responses in Human Myometrium. Scientific Reports2019.
46. Deshpande DA, Wang WC, McIlmoyle EL, et al. Bitter taste receptors on airway smooth muscle bronchodilate by localized calcium signaling and reverse obstruction. *Nat Med*. Nov 2010;16(11):1299-304. doi:10.1038/nm.2237
47. Luo M, Ni K, Jin Y, Yu Z, Deng L. Toward the Identification of Extra-Oral TAS2R Agonists as Drug Agents for Muscle Relaxation Therapies via Bioinformatics-Aided Screening of Bitter Compounds in Traditional Chinese Medicine. *Front Physiol*. 2019;10:861. doi:10.3389/fphys.2019.00861
48. Zheng K, Lu P, Delpapa E, et al. Bitter taste receptors as targets for tocolytics in preterm labor therapy. *FASEB J*. Sep 2017;31(9):4037-4052. doi:10.1096/fj.201601323RR
49. Norwitz ER, Caughey AB. Progesterone supplementation and the prevention of preterm birth. *Rev Obstet Gynecol*. 2011;4(2):60-72.
50. Fomin VP, Cox BE, Word RA. Effect of progesterone on intracellular Ca2+ homeostasis in human myometrial smooth muscle cells. *Am J Physiol*. Feb 1999;276(2):C379-85. doi:10.1152/ajpcell.1999.276.2.C379
51. Abbas Y, Carnicer-Lombarte A, Gardner L, et al. Tissue stiffness at the human maternal-fetal interface. *Hum Reprod*. 10 02 2019;34(10):1999-2008. doi:10.1093/humrep/dez139
52. Lyra-Leite DM, Andres AM, Petersen AP, et al. Mitochondrial function in engineered cardiac tissues is regulated by extracellular matrix elasticity and tissue alignment. *Am J Physiol Heart Circ Physiol*. Oct 1 2017;313(4):H757-H767. doi:10.1152/ajpheart.00290.2017
53. Alford PW, Nesmith AP, Seywerd JN, Grosberg A, Parker KK. Vascular smooth muscle contractility depends on cell shape. *Integr Biol (Camb)*. Nov 2011;3(11):1063-70. doi:10.1039/c1ib00061f

54. Flake GP, Moore AB, Sutton D, et al. The natural history of uterine leiomyomas: light and electron microscopic studies of fibroid phases, interstitial ischemia, inanosis, and reclamation. *Obstet Gynecol Int*. 2013;2013:528376. doi:10.1155/2013/528376
55. Jamaluddin MFB, Nahar P, Tanwar PS. Proteomic Characterization of the Extracellular Matrix of Human Uterine Fibroids. *Endocrinology*. Jul 01 2018;159(7):2656-2669. doi:10.1210/en.2018-00151
56. Winter A, Salamonsen LA, Evans J. Modelling fibroid pathology: development and manipulation of a myometrial smooth muscle cell macromolecular crowding model to alter extracellular matrix deposition. *Mol Hum Reprod*. 07 01 2020;26(7):498-509. doi:10.1093/molehr/gaaa036
57. Luca AM, Carvalho JCA, Ramachandran N, Balki M. The effect of morbid obesity or advanced maternal age on oxytocin-induced myometrial contractions: an in vitro study. *Can J Anaesth*. 07 2020;67(7):836-846. doi:10.1007/s12630-020-01615-6
58. Balki M, Kanwal N, Erik-Soussi M, Kingdom J, Carvalho JC. Contractile efficacy of various prostaglandins in pregnant rat myometrium pretreated with oxytocin. *Reprod Sci*. Sep 2012;19(9):968-75. doi:10.1177/1933719112438971
59. Pehlivanoğlu B, Bayrak S, Doğan M. A close look at the contraction and relaxation of the myometrium; the role of calcium. *Journal of the Turkish German Gynecological Association*. 2013;14(4):230-234. doi:10.5152/jtgga.2013.67763
60. Norian JM, Owen CM, Taboas J, et al. Characterization of tissue biomechanics and mechanical signaling in uterine leiomyoma. *Matrix Biol*. Jan 2012;31(1):57-65. doi:10.1016/j.matbio.2011.09.001
61. Harrod JS, Rada CC, Pierce SL, England SK, Lamping KG. Altered contribution of RhoA/Rho kinase signaling in contractile activity of myometrium in leptin receptor-deficient mice. *Am J Physiol Endocrinol Metab*. Aug 2011;301(2):E362-9. doi:10.1152/ajpendo.00696.2010
62. Sato H, Kato R, Isogai Y, et al. Analyses of group III secreted phospholipase A2 transgenic mice reveal potential participation of this enzyme in plasma lipoprotein modification, macrophage foam cell formation, and atherosclerosis. *J Biol Chem*. Nov 28 2008;283(48):33483-97. doi:10.1074/jbc.M804628200
63. Zhang CH, Lifshitz LM, Uy KF, Ikebe M, Fogarty KE, ZhuGe R. The cellular and molecular basis of bitter tastant-induced bronchodilation. *PLoS Biol*. 2013;11(3):e1001501. doi:10.1371/journal.pbio.1001501
64. Tuzim K, Korolczuk A. An update on extra-oral bitter taste receptors. *J Transl Med*. Oct 21 2021;19(1):440. doi:10.1186/s12967-021-03067-y
65. Gnecco JS, Pensabene V, Li DJ, et al. Compartmentalized Culture of Perivascular Stroma and Endothelial Cells in a Microfluidic Model of the Human Endometrium. *Ann Biomed Eng*. Jul 2017;45(7):1758-1769. doi:10.1007/s10439-017-1797-5
66. Pemathilaka RL, Caplin JD, Aykar SS, Montazami R, Hashemi NN. Placenta-on-a-Chip: In Vitro Study of Caffeine Transport across Placental Barrier Using Liquid Chromatography Mass Spectrometry. *Glob Chall*. Mar 2019;3(3):1800112. doi:10.1002/gch2.201800112
67. Aziz AUR, Yu X, Jiang Q, et al. Doxorubicin-induced toxicity to 3D-cultured rat ovarian follicles on a microfluidic chip. *Toxicol In Vitro*. Feb 2020;62:104677. doi:10.1016/j.tiv.2019.104677